Journal of Neurochemistry

JOURNAL OF NEUROCHEMISTRY | 2018 | 145 | 245–257 doi: 10.1111/jnc.14295

ORIGINAL ARTICLE

A dual role for Integrin α6β4 in modulating hereditary neuropathy with liability to pressure palsies

Yannick Poitelon,*,†,[1] Vittoria Matafora,‡,[2] Nicholas Silvestri,§ Desirée Zambroni,‡ Claire McGarry,† Nora Serghany,† Thomas Rush,† Domenica Vizzuso,*,‡ Felipe A. Court,‡,¶ Angela Bachi,‡ Lawrence Wrabetz*,†,‡,§ and Maria Laura Feltri*,†,‡,§

*Hunter James Kelly Research Institute, University at Buffalo, Buffalo, New York, USA
†Department of Biochemistry, University at Buffalo, Buffalo, New York, USA
‡Division of Genetics and Cell Biology, San Raffaele Hospital, Milan, Italy
§Department of Neurology, University at Buffalo, Buffalo, New York, USA
¶Center for Integrative Biology, Universidad Mayor de Chile, Santiago, Chile

Abstract

Peripheral myelin protein 22 (PMP22) is a component of compact myelin in the peripheral nervous system. The amount of PMP22 in myelin is tightly regulated, and PMP22 over or under-expression cause Charcot-Marie-Tooth 1A (CMT1A) and Hereditary Neuropathy with Pressure Palsies (HNPP). Despite the importance of *PMP22*, its function remains largely unknown. It was reported that *PMP22* interacts with the β4 subunit of the laminin receptor α6β4 integrin, suggesting that α6β4 integrin and laminins may contribute to the pathogenesis of CMT1A or HNPP. Here we asked if the lack of α6β4 integrin in Schwann cells influences myelin stability in the HNPP mouse model. Our data indicate that PMP22 and β4 integrin may not interact directly in myelinating Schwann cells, however, ablating β4 integrin delays the formation of tomacula, a characteristic feature of HNPP. In contrast, ablation of integrin β4 worsens nerve conduction velocities and non-compact myelin organization in HNPP animals. This study demonstrates that indirect interactions between an extracellular matrix receptor and a myelin protein influence the stability and function of myelinated fibers.

Keywords: HNPP, Integrin β4, myelin, peripheral nerve, Pmp22, Schwann cells.

J. Neurochem. (2018) **145**, 245–257.

Peripheral myelin protein 22 (PMP22) is a constituent of peripheral myelin (Welcher *et al.* 1991). Defects in PMP22 gene dosage cause the most common inherited diseases of peripheral nerves, which includes Hereditary Neuropathy with liability to Pressure Palsies (HNPP), due to deletion of a genetic region containing the PMP22 allele (Chance *et al.* 1993). Mice haploinsufficient for PMP22 recapitulate human HNPP pathology, that includes the formation of tomacula (smooth thickening of myelin typically at paranodes), progressive demyelination and failure of action potential propagation (Adlkofer *et al.* 1995, 1997; Bai *et al.* 2010). Although *PMP22* was identified 25 years ago, the function of PMP22 in myelin remains mysterious (Snipes *et al.* 1992). PMP22 may participate in actin-mediated cellular functions and in establishing lipid rafts (Lee *et al.* 2014). Other hypotheses regarding its function include compact myelin stabilization (D'Urso *et al.* 1999; Hasse *et al.* 2004), the promotion of Schwann cell differentiation, proliferation or apoptosis (Fabbretti *et al.* 1995; Sancho *et al.* 2001; Amici *et al.* 2007), calcium homeostasis (Nobbio *et al.* 2009) and

Received July 25, 2017; revised manuscript received December 14, 2017; accepted December 21, 2017.

Address correspondence and reprint requests to Maria Laura Feltri, Hunter James Kelly Research Institute, University at Buffalo, Buffalo, New York 14203, USA. E-mail: mlfeltri@buffalo.edu

[1]Present addresses: Albany Medical College, Albany, New York 12208, USA.

[2]IFOM-FIRC Institute of Molecular Oncology, Milan 20139, Italy

Abbreviations used: HNPP, hereditary neuropathy with pressure palsy; NCV, nerve conduction velocities; SC, Schwann cell.

maintenance of myelin permeability (Guo *et al.* 2014; Hu *et al.* 2016). β4 integrin interacts with the α6 integrin subunit to form a laminin receptor that provides stability and mechanical support to myelinated fibers (Feltri *et al.* 1994; Quattrini *et al.* 1996; Nodari *et al.* 2008),

During early stages of myelination, PMP22 and α6β4 integrin are co-expressed in Schwann cells and can be co-immunoprecipitated (Amici *et al.* 2006), but while PMP22 is present in compact myelin, α6β4 integrin is on the outer layer of the Schwann cell membrane. Therefore, it is uncertain how and where the interaction between PMP22 and α6β4 integrin may occur in nerves. Finally, deletion of *Pmp22* or β4 integrin causes similar pathological features, but with drastically different age of onset, as *Pmp22* haploinsufficient animals develop tomacula between 10 and 20 days of age (Adlkofer *et al.* 1995, 1997) and mice with β4 integrin deletion in Schwann cells develop myelin folding and demyelination at 12 months (Quattrini *et al.* 1996; Nodari *et al.* 2008).

To elucidate the significance of the interaction between PMP22 and α6β4 integrin, we performed careful co-localization and biochemical analysis and identified novel interactors of the β4 integrin subunit. To ask if the lack of α6β4 integrin in Schwann cells influences myelin stability in the HNPP model, we generated mice lacking both PMP22 and β4 integrin in Schwann cells. We find that ablation of β4 integrin in HNPP does not modify myelin thickness or internodal length and does not worsen abnormal myelin folding, but worsens nerve conduction velocities in HNPP animals, and this correlates with worsening of the paranodal and internodal disorganization. These data indicate that integrin α6β4 and PMP22 cooperate to organize the internode and to allow proper propagation of the axonal signal along the axons.

Methods

Animal models and genotyping

All animal procedures were performed in accordance with San Raffaele Institute and University at Buffalo animal care committee regulations (n. 363 and UB1188M, respectively). *Itgb4* floxed mice (RRID:MGI:3804178), *Pmp22* knock-out mice (RRID:MGI:3794448) and P0-Cre transgenic mice (RRID:IMSR_JAX:017927) have been described previously (Adlkofer *et al.* 1995; Feltri *et al.* 1999; Nodari *et al.* 2008). Animal's references can be retrieved with RRIDs at http://scicrunch.org/resources. Animals used as controls are *Pmp22* +/+; *Itgb4* fl/fl; P0-cre negative (*Pmp22* +/+; *Itgb4* SC +/+). *Pmp22* +/- animals are *Pmp22* +/-; *Itgb4* fl/fl; P0-Cre negative (*Pmp22* +/-; *Itgb4* SC +/+). *Itgb4* SC -/- animals are *Itgb4* fl/fl; P0-Cre positive (*Pmp22* +/+; *Itgb4* SC -/-). Finally, *Pmp22* +/-; *Itgb4* SC -/- animals are *Pmp22* +/-; *Itgb4* fl/fl; P0-Cre positive (*Pmp22* +/-; *Itgb4* SC -/-). All mice were backcrossed to C57BL/6 to reach congenic background. Both males and females were included in the study. Mutant and control littermates were killed at the indicated ages, and sciatic nerves were dissected. No animals were excluded from the study. Animals were housed in cages of no more than five animals in 12 h light/dark cycles. Most experiments were conducted with three animals per age and per genotype. A flowchart of the experimental procedures is available in Fig. S5. Genotyping of mutant mice was performed by PCR on tail genomic DNA, as described previously (Adlkofer *et al.* 1995; Feltri *et al.* 1999; Nodari *et al.* 2008).

Electrophysiology

Animals were analyzed at 30 days of age as described previously (Poitelon *et al.* 2015). Briefly, mice were anesthetized with tribromoethanol, 0.02 mL/g of body weight, and placed under a heating lamp to avoid hypothermia. Sciatic nerve motor conduction velocity and amplitude were obtained with subdermal steel monopolar needle electrodes: a pair of stimulating electrodes was inserted subcutaneously near the nerve at the ankle, then at the sciatic notch, and finally at the paraspinal region at the level of the iliac crest to obtain three distinct sites of stimulation, proximal and distal, along the nerve. Compound motor action potential were recorded with an active electrode inserted in muscles in the middle of the paw and a reference needle in the skin between the first and second digits.

Morphological assessments

Mutant and control littermates were killed at the indicated ages, and sciatic nerves were dissected. Tissues were fixed in 2% buffered glutaraldehyde and post-fixed in 1% osmium tetroxide. After alcohol dehydration, the samples were embedded in Epon. Transverse sections (0.5–1 nm thick) were stained with toluidine blue and examined by light microscopy. Morphological measurements were quantified from anatomically comparable whole cross section of sciatic nerve cut halfway between the sciatic notch and the knee. For G-ratio analysis of sciatic nerves (axon diameter/fiber diameter), four images per semithin section were acquired at the 100× objective. Axon and fiber diameters were quantified using the Leica QWin software (Leica Microsystem, Wetzlar, Germany). Myelinated fibers and tomacula were quantified on the whole cross section of sciatic nerve using ImageJ (imagej.nih.gov/ij). Data were analyzed using GraphPad Prism (GraphPad Software, La Jolla, CA, USA) 6.01. Images were quantified blindly.

Teasing and osmication of nerve fibers

Sciatic nerves were fixed in 2% glutaraldehyde overnight at 4°C and washed three times in phosphate buffer (79 mM Na_2HPO_4, 21 mM NaH_2PO_4, pH 7.4). Sciatic nerves were stained in 1% osmium, washed four times in phosphate buffer and incubated at 55°C during 12 h in 30% glycerol followed by 12 h in 60% glycerol and 12 h in 100% glycerol.

Immunoelectron microscopy

Immuno-electron microscopy analyses were performed as in (Quattrini *et al.* 1996), but with embedding modified as described in (Yin *et al.* 2000). Primary antibody to PMP22 (Abcam, Cambridge, United Kingdom, ab61220, RRID:AB_944897), and 5 nM of gold conjugated secondary antibody were used. Immunoelectron microscopy analysis was performed once.

Cell culture

Rat 804G (RRID:CVCL_J122) and hamster CHO (RRID:CVCL_0213) cells were maintained in Dulbecco's modified Eagle's

medium (Gibco, Gaithersburg, MD, USA), 10% fetal calf serum (FCS), penicillin and streptomycin. 804G permanently transfected with β4 integrin mutants were a gift from Dr Giancotti (Spinardi *et al.* 1993). Transfection of HA-Pmp22 and β4 integrin were performed using Lipofectamine 2000 (Invitrogen, Carlsbad, CA, USA), according to the manufacturer's instructions. Cells were analyzed 72 h after transfection to insure efficient expression of the transfected plasmids. Each transfection was repeated at least three times.

Western blot

Sciatic nerves were dissected, removed from their epineurium, frozen in liquid nitrogen then pulverized. Transfected hamster CHO cells (RRID:CVCL_0213) and sciatic nerves were resuspended in lysis buffer (95 mM NaCl, 25 mM Tris-HCl pH 7.4, 10 mM EDTA, 2% sodium dodecyl sulfate (SDS), 1 mM Na_3VO_4, 1 mM NaF and 1 : 100 Protease Inhibitor Cocktail, Roche Molecular Biochemicals, Basel, Switzerland). Protein lysates were incubated at 4°C for 30 min then centrifuged at 13 000 g for 30 min at 4°C. The concentration of the protein supernatants was determined by bicinchoninic acid protein assay (Thermo Scientific, Waltham, MA, USA) according to manufacturer's instructions. Equal amounts of homogenates were diluted 3 : 1 in 4 × Laemmli (250 mM Tris-HCl pH 6.8, 8% SDS, 8% β-Mercaptoethanol, 40% Glycerol, 0.02% Bromophenol Blue), denatured 5 min at 100°C, resolved on SDS-polyacrylamide gel, and electroblotted onto polyvinylidene difluoride membrane. Blots were then blocked with 5% bovine serum albumin in 1 × phosphate-buffered saline (PBS), 0.05% Tween-20 and incubated over night with the appropriate antibody. Abcam anti-PMP22 (ab61220, RRID:AB_944897), Cell Signaling Technology, Danvers, MA, USA anti-PAK1 (2602, RRID:AB_330222), GenWay, San Diego, CA, USA anti-p-PAK1 (GWB-961E2C, RRID:AB_10275529), Millipore, Burlington, MA, USA anti-integrin β1 (MAB1997, RRID:AB_2128202), anti-Itpr3 (AB9076, RRID:AB_571029), Novocastra, Newcastle, United Kingdom anti-β-dystroglycan (NCL-b-DG, RRID:AB_442043), Roche anti-HA (11867423001, RRID:AB_390918), Santacruz, Dallas, TX, USA anti-integrin β4 human (sc-9090, RRID:AB_2129021), anti-integrin α6 (sc-6597, RRID:AB_2128041) and Sigma anti-β-tubulin (T4026, RRID:AB_477577), anti-calnexin (C4731, RRID:AB_476845). Antibodies references can be retrieved with RRIDs at http://scicrunch.org/resources. Anti-integrin β4 mouse/rat (lot 2213) was gift of Dr Brophy, Centre for Neuroregeneration, Univ. of Edinburgh). Membranes were rinsed in 1 × PBS and incubated for 1 h with secondary antibodies. Blots were developed using ECL, ECL plus (GE Healthcare, Little Chalfont, United Kingdom) or Odyssey CLx infrared imaging system (Li-Cor Bioscience, Lincoln, NE, USA). Western blots were quantified using Image J software (http://imagej.nih.gov/ij). Each western blot was repeated at least three times.

Immunoprecipitation

Rat 804G cells and sciatic nerves fibers were resuspended in lysis buffer (150 mM NaCl, 50 mM Tris-HCl pH 7.4, 0.5% Sodium deoxycholate, 1% NP-40, 1 : 100 Protease Inhibitor Cocktail, Roche). For each immunoprecipitation, 500 µg of proteins was incubated with 50 µL of Protein G Sepharose for 1 h at 4°C on a rotating wheel. After a short centrifugation, supernatants were transferred to a new vial, incubated overnight at 4°C with 1 µg of antibody [Abcam anti-Integrin β4 (ab25254, RRID:AB_2129042) or Roche anti-HA (11867423001, RRID:AB_390918)] on a rotating wheel. 50 µL of Protein G Sepharose was added to the mix and incubated for an additional 3 h. After centrifugation, supernatants were collected as unbound fraction (Ub), pellets were washed three time in lysis buffer, resuspended in Laemmli and processed as western blot as the immunoprecipitated fraction (IP). Equal amounts of proteins were incubated with the target antibody, precipitated, separated by SDS/sodium dodecyl sulfate–polyacrylamide gel electrophoresis (PAGE) and probed. Each immunoprecipitation was repeated at least three times.

Immunohistochemistry

We tested various fixation and anti-PMP22 antibodies against nerves from *Pmp22* −/− animals at various ages. Surprisingly, numerous antibodies anti-PMP22 (Abcam ab126769, RRID:AB_11129961; Assay Biotech, Fremont, CA, USA C0306, RRID:AB_10686127; LifeSpan, Providence, RI, USA, LS-C118559-100, RRID:AB_10796545; LS-C122324-100, RRID:AB_10799898; Santacruz sc-58572, RRID:AB_785236; sc-18535, RRID:AB_2167000; sc-71911, RRID:AB_2167001; sc-65739, RRID:AB_2167002; Sigma-Aldrich (St. Louis, MO, USA) SAB4502217, RRID:AB_10746275) gave positive stainings in all conditions tested even in null tissues, and were not further pursued. Only one anti-PMP22 (ab61220, RRID:AB_944897) showed no PMP22 signal in SCs of $PMP22^{-/-}$ animals (Fig. S4). The antibodies references can be retrieved with RRIDs at http://scicrunch.org/resources. The following conditions gave no background staining for PMP22 in *Pmp22*−/− null animals (data not shown). Unfixed sciatic nerve sections and sciatic nerve teased fibers were fixed with cold methanol for 1 min or cold acetone for 10 min, washed in 1 × PBS, blocked for 1 h in blocking solution (5% Fish skin gelatin, 0.5% Triton X-100, 1 × PBS), then incubated overnight with the following antibodies: Abcam anti-Integrin β4 (ab25254, RRID:AB_2129042), anti-PMP22 (ab61220, RRID:AB_944897), Alomone labs, Jerusalem, Israel anti-Kv1.1 (APC-009, RRID:AB_2040144), Covance, Princeton, NJ, USA anti-Neurofilament M (PCK-593P, RRID:AB_663194), Millipore anti-Integrin β1 (MAB1997, RRID:AB_2128202), Invitrogen Rhodamine Phalloidin (R415, RRID:AB_2572408), Santacruz anti-Integrin α6 (sc-6597, RRID:AB_2128041), Sigma anti-Itpr3 (AB9076, RRID:AB_571029), anti-Claudin-19 was a gift by Dr Shoichiro Tsukita and Dr Mikio Furuse. Slides were rinsed in PBS, incubated 1 h with Jackson DyLight 488 or 549-conjugated secondary antibodies, stained with 4′,6-diamidino-2-phenylindole (DAPI), and mounted with Vectashield (Vector Laboratories, Peterborough, United Kingdom). Images were acquired with an upright microscope Leica DM5000, a Zeiss (Oberkochen, Germany) Apotome or a confocal microscope Leica SP5II. Each immunochemistry was repeated at least three times.

Proximity ligation assay

Unfixed sciatic nerve sections were fixed in cold methanol for 1 min, washed in in 1 × PBS then blocked for 1 h in blocking solution (5% Fish skin gelatin, 0.5% Triton X-100, 1 × PBS). Slides were then incubated overnight with the following antibodies: Abcam anti-Integrin β4 (ab25254, RRID:AB_2129042) and anti-PMP22 (ab61220, RRID:AB_944897) or Millipore anti-Neurofilament M (MAB-10651, RRID:AB_2150076) and anti-Neurofilament H (AB1989, RRID:AB_91202). MINUS probe was coupled to anti-Integrin β4 using *In Situ* Probemaker (Sigma). The following

procedures were carried out using the Duolink starter kit (Sigma) products. Proximity ligation assay probes PLUS (rabbit) and MINUS (mouse) were diluted 1 : 5 in blocking solution and incubated 1 h at 37°C. Slides were washed twice in Wash Buffer A for 2 min. Ligase and ligation buffer were diluted 1 : 40 and 1 : 5 were diluted in 1 × PBS, and incubated on slides at 37°C for 30 min. Slides were washed twice in Wash Buffer A for 2 min. Polymerase and amplification buffer were diluted 1 : 80 and 1 : 5 in 1 × PBS, and incubated on slides at 37°C for 120 min. Slides were washed three time in Wash Buffer B for 10 min. Cells were stained with DAPI, and mounted with media supplied by the kit. Images were acquired with an upright microscope Leica DM5000. The proximity ligation assay was performed twice.

Quantitative real-time PCR

For quantitative real-time PCR, we sampled sciatic nerves from control and mutant mice at P5, P10, P30, and P90. Sciatic nerves were frozen in liquid nitrogen, crushed with a metallic pestle and total RNAs were isolated from sciatic nerve using TRIzol (Life Technologies, Carlsbad, CA, USA). First-strand cDNA was prepared from 1 μg or RNA using Superscript II, 50 μM oligo$(dT)_{20}$ and 50 ng random hexamers, according to the manufacturer's instructions. quantitative real-time PCR was performed using Sybr Green (Roche) in a LightCycler 480 System (Roche) according to standard protocols. Normalization was performed using 18S rRNA as a reference gene. The relative standard curve method was applied using wild-type mice as reference. At least three animals were used for each genotype at each age. Primers were designed with the Roche Primer Design Center (http://qpcr.probefinder.com/organism.jsp) and their efficiency was assessed by standard curve. Only primers 90% efficient or above were selected. Primer dimerization was tested *in vitro* by Amplify X (http://engels.genetics.wisc.edu/amplify) and the homogeneity of the PCR products was assessed by a dissociation curve. We used the following primers to amplify *18S*: 5′ ctcaacacgggaaacctcac 3′ and 3′ cgctccaccaactaagaacg 5′, *Egr2:* 5′ ctacccggtggaagacctc 3′ and 3′ aatgttgatcatgccatctcc 5′ *Itga6*: 5′ cctgaaagaaaataccagactctca 3′ and 3′ ggaacgaagaacgagagagg 5′, *Itga7*: 5′ agaaggtggagcctagcaca 3′ and 3′ gctgaacaccacacacttgg 5′, *Itgb1*: 5′ caaccacaacagctgcttctaa 3′ and 3′ tcagccctcttgaattttaatgt 5′, *Itgb4*: 5′ cttggtcgccgtctggta 3′ and 3′ tcgaaggacactaccccact 5′, *Mpz*: 5′ gctgccctgctcttctctt 3′ and 3′ tttccctgtccg tgtaaacc 5′, *Pmp22*: 5′ ccgtccaacactgctactcc 3′ and 3′ cgctgaagatgacagacagg 5′. Each quantitative real-time PCR was repeated twice.

Mass spectrometry and data analysis

Immunoprecipitated eluates were separated by 4–12% sodium dodecyl sulfate–polyacrylamide gel electrophoresis, stained with Coomassie Brilliant Blue (Bio-Rad Laboratories, Hercules, CA, USA) and excised in eight slices for LC-MS/MS analysis. Mass spectrometry analysis was performed by LC-MS/MS using an LTQ-Orbitrap mass spectrometer (ThermoScientific, Bremen, Germany). Tryptic digests for each band were first cleaned using Stage Tips as described previously (Rappsilber *et al.* 2007) and then injected in a capillary chromatographic system (EasyLC, Proxeon Biosystems, Odense, Denmark). Peptide separations occurred on a homemade column obtained with a 10-cm fused silica capillary (75 μm inner diameter and 360 μm outer diameter; Proxeon Biosystems) filled with Reprosil-Pur C18 3 μm resin (Dr Maisch GmbH, Ammerbuch-Entringen, Germany) using a pressurized 'packing bomb'. A gradient of eluents A [distilled water with 2% (v/v) acetonitrile, 0.1% (v/v) formic acid] and B [acetonitrile, 2% (v/v) distilled water with 0.1% (v/v) formic acid] was used to achieve separation from 8% B (at 0 min, 0.2 mL/min flow rate) to 50% B (at 80 min, 0.2 mL/min flow rate). The LC system was connected to the orbitrap equipped with a nanoelectrospray ion source (Proxeon Biosystems). Full-scan mass spectra were acquired in the LTQ-Orbitrap mass spectrometer in the mass range m/z 350–1500 Da and with the resolution set to 60 000. The 'lock-mass' option was used for accurate mass measurements. The 10 most intense doubly and triply charged ions were automatically selected and fragmented in the ion trap. Target ions already selected for the MS/MS were dynamically excluded for 60 s (Olsen *et al.* 2005). Protein identification and quantification were achieved using the MaxQuant software version 1.3.0.5 (Cox and Mann 2008). Cysteine carbamidomethylation was searched as a fixed modification, whereas *N*-acetyl protein and oxidized methionine were searched as variable modifications. Mass spectra were analyzed by Andromeda plugin in MaxQuant using UniProt complete proteome Mus musculus 2013 database. Protein quantification was based on label free quantitation (LFQ) intensities. Peptides and proteins were accepted with a false-discovery rate of 0.01, two minimum peptides identified per protein of which one unique. The experiments were done in biological duplicate performing two technical replicates.

Gene ontology analysis

Gene ontology (GO) clustering analysis was performed using the Cytoscape (http://chianti.ucsd.edu/cyto_web/plugins/index.php) plugin Biological Network Gene Ontology (BiNGO) (http://www.psb.ugent.be/cbd/papers/BiNGO/index.html). The degree of functional enrichment for a given cluster and category was assessed quantitatively (P value) by hypergeometric distribution, a multiple test correction was applied using the false-discovery rate algorithm, fully implemented in BiNGO software. Overrepresented biological process categories were generated after false discovery rate correction, with a significance level of 0.05. The full analysis is listed in Data S3.

Statistical analyses

Experiments were not randomized, but data collection and analysis were performed blindly to the conditions of the experiments. Researchers blinded to the genotype performed morphological analyses, nerve conduction velocities and morphometric analyses. The data obtained are presented as mean ± SEM. No statistical methods were used to predetermine sample sizes, but our sample sizes are similar those generally employed in the field. t-test and one-way ANOVA with Bonferroni's multiple comparisons test were used for statistical analysis of the differences among multiples groups according to the number of samples. Values of $p \leq 0.05$ were considered to represent a significant difference. This study was not preregistered.

Results

Ablation of integrin α6β4 has both beneficial and detrimental effects on the HNPP mouse model

To test for functional interactions between α6β4 integrin and PMP22, we asked whether α6β4 integrin in Schwann cells

modifies the timing or severity of myelin abnormalities associated with HNPP, exploiting an authentic model of *Pmp22* loss-of-function (Adlkofer *et al.* 1995; Bai *et al.* 2010) and the conditional, Schwann cell specific, knock-out for integrin β4 (Feltri *et al.* 1999; Nodari *et al.* 2008). We generated double mutant (*Pmp22* +/- and *Itgb4* SC−/−) animals and analyzed myelination in the peripheral nervous system.

Analysis of *Pmp22* +/- nerves by semithin sections from 20 to 90 days of age confirmed previous reports that haploinsufficiency of *Pmp22* does not cause axonal loss or early demyelination (Fig. 1a–d), but promotes the formation of tomacula (Fig. 1a arrows, Fig. 1g open arrows) and a reduction in the length of myelin internodes (Fig. 1g–i) (Adlkofer *et al.* 1995, 1997; Amici *et al.* 2007; Hu *et al.* 2016). Surprisingly, we observed that ablation of integrin α6β4 slightly delays the appearance of tomacula (Fig. 1e and f). A significant reduction in the number of tomacula can be observed at 20 days of age (P20) while myelination is ongoing, but disappears at P200 once myelin is mature (Fig. 1e). We also noticed a moderate increase in the length of myelin segments (internodes) in double mutants as compared to *Pmp22* +/- animals at P30 (Fig. 1g–i). The increase is significant for internodes of small caliber fibers (Fig. 1i). Together these data indicate that ablation of integrin α6β4 delays the onset of morphological defects caused by *Pmp22* haploinsufficiency.

In contrast, electrophysiological analyses in 1-month-old animals showed that ablation of α6β4 integrin worsens the nerve conduction velocities (NCV) of HNPP animals (Table 1). This was not because of a change in internodal length, which was increased in double mutants only in small myelinated fibers which do not contribute to NCVs (Li 2015) A. These data indicate that integrin α6β4 and PMP22 collaborate to allow proper propagation of the nervous signal along axons, in a way that is independent of myelin thickness (Fig. 1b) and of internodal length.

Overall, ablation of integrin α6β4 affects positively the HNPP phenotype by reducing the number of tomacula and restoring internodal length in small caliber fibers, but it also reduces NCV. While these observations are conflicting, they likely represent different pathogenic mechanisms of *Pmp22* haploinsufficiency, which are modulated differently by integrin α6β4.

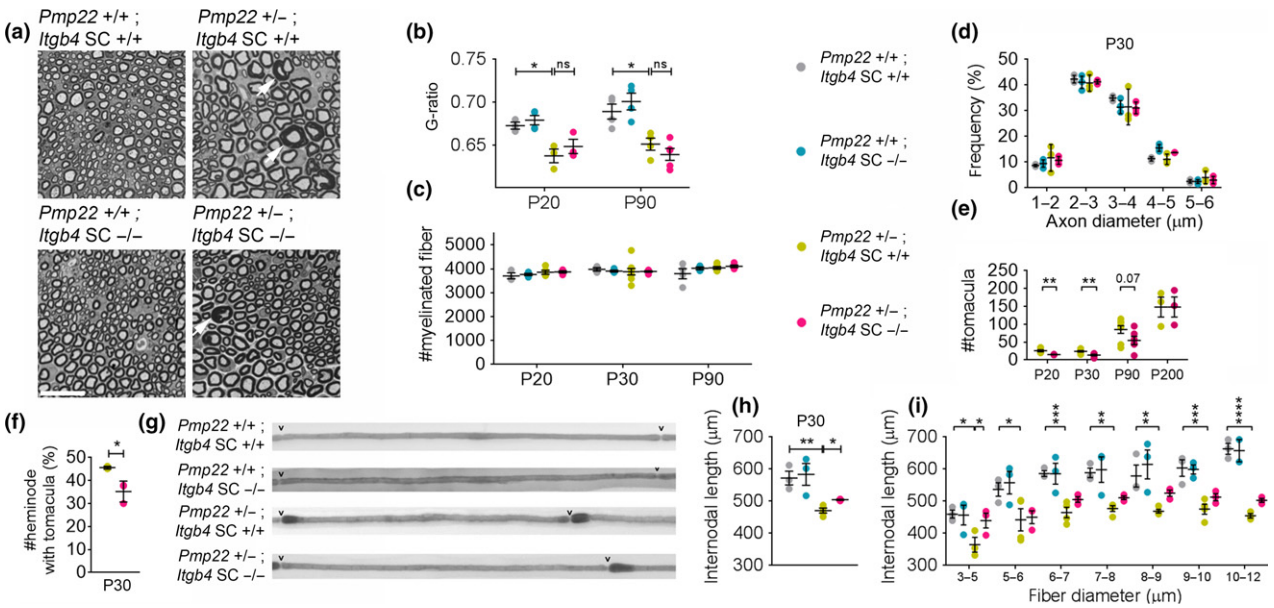

Fig. 1 Ablation of β4 integrin in Schwann cells delays the morphological defects of hereditary neuropathy with pressure palsy (HNPP). Schwann cell-specific deletion of β4 integrin delays the formation of tomacula and restores internodal length in HNPP mice at 30 days of age (P30). (a) Semithin cross-sections of sciatic nerves stained with toluidine blue from the indicated genotypes 30 days of age. Tomacula can be distinguished in *Pmp22* +/- and double mutants by their myelin thickening (arrows). Scale bar, 50 μm. (b) G ratio was decreased by 0.035 at P20 and 0.038 at P90 only in *Pmp22* +/- and not further modified by ablation of β4 integrin in Schwann cells. (c–e) Number of myelinated fibers at P20, P30 and P90 (c), axonal size distribution at P30 (d) and number of tomacula at P20, P30, P90 and P200 (e). Fibers were quantified from a whole semithin section of sciatic nerve. (f–g) Examples of paranodal tomacula in *Pmp22* +/- and double mutant animals are shown in (g), and their quantification in (f). The appearance of tomacula is slightly delayed in *Pmp22* +/-; *Itgb4* SC −/− sciatic nerves as compared to *Pmp22* +/+; *Itgb4* SC +/+ nerves. Internodal length (h–i) quantified from osmicated teased sciatic nerve fibers from at 30 days of age. Note that ablation of β4 integrin improves the shorter internodal length of *Pmp22* +/- animals (h), especially in small caliber fibers (i). All graphs indicate mean ± SEM n (animals) ≥ 3 per genotype (Data S1). Statistical analyses were performed using *t*-test with Bonferroni correction (b, d, f, h) and two-way ANOVA with Bonferroni *post hoc* test (i). $*p < 0.05$, $**p < 0.01$, $***p < 0.001$, $****p < 0.001$. n.s. indicates non-significant.

Table 1 Ablation of integrin β4 decreases nerve conduction velocities of HNPP animals

	Pmp22 +/+; *Itgb4* SC +/+	*Pmp22* +/+; *Itgb4* SC −/−	*Pmp22* +/-; *Itgb4* SC +/+	*Pmp22* +/-; *Itgb4* SC −/−
Conduction velocity (m/s)	43.38 ± 1.55	40.30 ± 2.62	33.06 ± 1.01	24.35 ± 0.5
	n.s.		$p = 0.0017$,	$p = 0.01$
cMAP amplitude (mV)	3.53 ± 0.38	2.84 ± 0.22	2.38 ± 0.12	2.88 ± 0.14
	n.s.		*n.s.*	*n.s.*
cMAP latency (ms)	1.28 ± 0.04	1.50 ± 0.15	1.75 ± 0.05	1.84 ± 0.02
	n.s.		$p = 0.0058$	n.s.

Electrophysiological analysis of animals at 30 days of age. The analysis reveals a decrease of NCV (43.85 m/s vs. 33.06 m/s) and an increase of latency (1.28 vs. 1.75 ms) in *Pmp22* +/- animals. Additional ablation of β4 integrin further decreased the NCV (24.54 m/s). ± indicate SEM. Statistical analysis was performed using one-way ANOVA. n.s. indicates non-significant. $n \geq 7$ nerves per genotype (Data S1).

Integrin α6β4-PMP22 do not co-localize in myelinating Schwann cells

Because integrin α6β4 is present at the outer Schwann cell membrane (Einheber *et al.* 1993; Feltri *et al.* 1994), while PMP22 is localized in compact myelin (Haney *et al.* 1996) (see also Fig. S1), we hypothesized that the two proteins could interact in mature myelinated fibers in trans. We confirmed that integrin α6β4 and PMP22 can be co-immunoprecipitated from lysates of sciatic nerves at P30, as reported (Amici *et al.* 2006), and that this interaction is lost in PMP22-null or β4 integrin SC-null mice (Fig. 2a). However, using cell lines expressing various truncated forms of β4 integrin and transfected with an HA-PMP22 plasmid, we found that all truncated forms of β4 integrin appear to bind PMP22 (Fig. 2c). These data indicate that the two proteins do not interact in trans, but they could interact in cis via the only domain of β4 integrin that was not deleted, namely the transmembrane domain (i.e. amino acid 661-853) (Fig. 2d). From three distinct immunohistochemical approaches (i.e. proximity ligation assay, immunohistochemistry on sciatic nerve cross sections and on teased fibers), we showed that integrin α6β4 does not co-localize with PMP22 in the outer layer of the Schwann cell nor in compact myelin at P30 or as early as P3 (Fig. 2e–h, Fig S2, Data S2).

The discordance between the presence of co-immunoprecipitation from sciatic nerve lysates, the absence of co-localization and the persistence of co-immunoprecipitation in clones lacking most of the β4 integrin domains, may indicate that the interaction between integrin α6β4 and PMP22 is artefactual, and occurs in cell lysates, but not *in vivo*. This alternative explanation is supported by the observation that the interaction between β4 integrin and PMP22 can occur *in vitro*, after solubilization and mixing of the two proteins from two independent lysates, as shown in Fig. 2b. Overall, because we could not identify a specific β4 integrin domain of interaction with PMP22, nor could co-localize the two proteins in myelinating Schwann cells, we conclude that the two molecules probably do not physically interact in myelinating Schwann cells *in vivo*.

Ablation of integrin α6β4 increases PMP22 protein levels

Even if PMP22 and integrin α6β4 do not interact directly, the modification of the HNPP phenotype observed in *Pmp22* +/-; *Itgb4* SC −/− mice supports the existence of a functional interaction between the two proteins. We thus asked if ablation of β4 integrin affects the expression of *Pmp22*. We did not observe an effect on the mRNA levels of *Pmp22* or the myelin related genes *Egr2* and *Mpz*

Fig. 2 β4 integrin and PMP22 co-immunoprecipitate, but do not co-localize in myelinating Schwann cells. (a) Immunoprecipitation of β4 integrin in wild type, *Itgb4* SC −/− and *Pmp22* −/− sciatic nerves at 30 days of age. The data show that PMP22 immunoprecipitates with β4 integrin in wild type sciatic nerves, but not in nerves lacking either β4 integrin or PMP22. I = input, IP = immunoprecipitation and Ub = unbound fraction. (b) Post-lysis immunoprecipitation of PMP22 and β4 integrin**.** Human β4 integrin or HA-PMP22 were transfected independently into separate populations of CHO cells. The left panel is a western blot of the CHO cells transfected either with β4 integrin or with PMP22. The right panel is an immunoprecipitation performed from lysates of cells transfected only with integrin β4 subunit, only with HA-PMP22, or from a mix of the two lysates. The data show the interaction of PMP22 and β4 integrin detected *in vitro* after lysis of the cells. (c-d) Immunoprecipitation of PMP22 with various truncated forms of β4 integrin. 804G cell lines that stably express the truncated forms of human β4 integrin (cl. A-F) were transfected with HA-PMP22. The various truncated forms of β4 integrin (red) are depicted in (d) while interacting with the α6 integrin subunit (blue). All the truncated forms of β4 integrin interact with PMP22. cl.Ø does not express β4 integrin. (e) Proximity ligation assay (PLA) of β4 integrin and PMP22. Proximity ligation assay generates a signal (red dots) only if two proteins are in close vicinity (< 30 nm). The analysis does not detect close localization between β4 integrin and PMP22. (f) Immunolocalization of α6β4 integrin and PMP22 in teased fibers (f) and cross-sections (g–h) of sciatic nerve at 3 days (h) and 30 (f–g) days of age. Sections were stained for PMP22 (green), α6β4 integrin (red) and DAPI (blue). The data show that α6β4 integrin does not co-localize with PMP22 in adult myelinated Schwann cells. (Enlarged figures are displayed in Figure S2. A z-stack movie of a teased fiber is displayed in Data S2). Images were acquired with an apotome or a confocal microscope. Scale bar, 50 μm (e), 20 μm (f), 5 μm (g and h).

(Fig. 3a). However, the protein levels of PMP22 were modestly increased by 25% in *Pmp22* +/+; *Itgb4* SC −/− and in double mutant animals (Fig. 3b). Conversely, it was shown that absence of PMP22 could affect the expression and organization specifically of the α6β4 integrin basal lamina receptor (Amici *et al.* 2006, 2007). Thus, we asked if *Pmp22* haploinsufficiency could affect the expression of α6β4 integrin or other basal lamina receptors. However, we

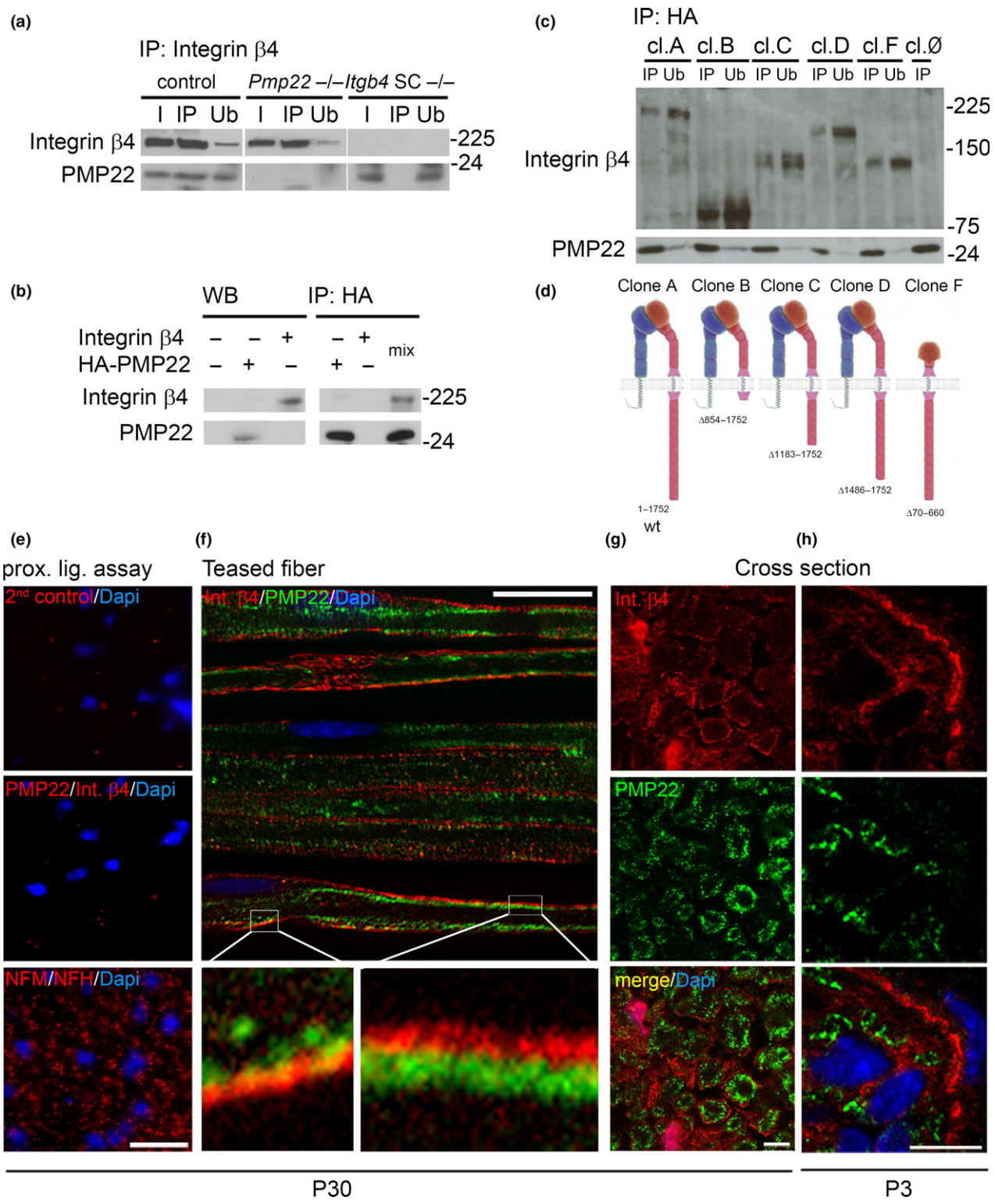

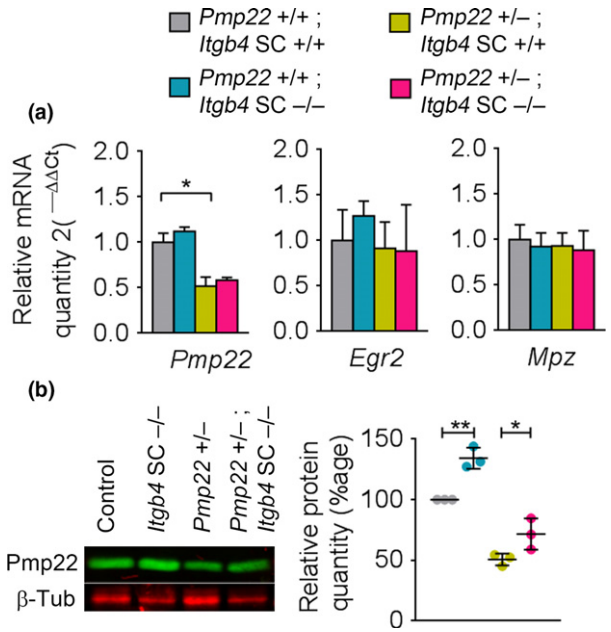

Fig. 3 PMP22 protein levels are increased in *Pmp22* +/-; *Itgb4* SC –/– sciatic nerves. (a and b) mRNA (a) and protein (b) levels for *Pmp22*, *Egr2* and *Mpz* were assessed in sciatic nerves of the indicated genotypes at 30 days of age. *Pmp22* mRNA and protein levels are reduced by 50% in *Pmp22* +/-. Ablation of *Itgb4* does not affect *Pmp22*, *Egr2*, *Mpz* mRNA levels, but causes an increase in the levels of PMP22 protein. Also, ablation of *Pmp22* does not affect the protein levels or the localization of laminin receptors (Fig. S3). Graphs indicate mean ± SEM n (animals) = 3 per genotype (Data S1). Statistical analyses were performed using *t*-test (a) and one-way ANOVA with Bonferroni *post hoc* test (b). $*p < 0.05$, $**p < 0.01$.

did not observe any difference in the mRNA, protein levels, or localization of any laminin receptors in HNPP sciatic nerves (Fig. S3).

NCV defects can be because of thinner myelin, shorter internodes, smaller axons, alterations in the electrical properties of myelin owing to imbalanced lipid composition or abnormal paranodal axoglial junctions (Coetzee *et al.* 1996; Dupree *et al.* 1998; Court *et al.* 2004; Miyamoto *et al.* 2005; Sherman *et al.* 2005). We showed that there is no overall decrease in the number of myelinated fibers, internodal length or myelin thickness in *Pmp22* +/-; *Itgb4* SC –/– mice (Fig. 1). Therefore, it is possible that modifications of the NCVs are associated with other morphological features such as the electrical properties of the myelin sheath. Recently studies have reported that deficiency of *Pmp22* in HNPP causes abnormal myelin permeability, also called 'functional demyelination' (Guo *et al.* 2014; Hu *et al.* 2016). According to this model, the absence of *Pmp22* affects the formation of tight and adherens autotypic junctions during development, and causes an increase in p21-activated kinase (PAK1) (Guo *et al.* 2014; Hu *et al.* 2016). The combined haploinsufficiency of PMP22 with increased PAK1 levels then leads to a further disruption of autotypic junctions and of F-actin organization in animals older than 3 months (Hu *et al.* 2016). It is possible that the absence of α6β4 integrin aggravates or accelerates the defects associated with myelin permeability in HNPP nerves. To test this hypothesis, we analyzed the localization of F-Actin at Schmidt-Lanterman incisures, Claudin-19 at paranodes and Kv1.1 at juxtaparanodes. In 1-month-old sciatic nerves from *Pmp22* +/- *Itgb4* SC –/– animals, we did not observe mislocalization of these proteins (Fig. 4a–b and d). In 3-month-old animals, we confirmed that staining for F-Actin was increased in Schmidt–Lanterman incisures of PMP22 mutants (Fig. 4c and e), and ablation of β4 integrin alone did not affect the F-Actin localization. However, F-actin staining was increased in Schmidt-Lanterman incisures of PMP22 and double mutants at 3 months (Fig. 4e) and F-actin was more disorganized in numerous internodes of double mutants, both at 1-month and 3-months of age (Fig. 4c, white lines, Fig. 4f). We also analyzed the activation of PAK1 at 15 days and 3 months of age. We confirmed that p-PAK1 levels are increased in Pmp22 +/- mutants, by 30% at P15 and by 60% at P30 (Hu *et al.* 2016), and this appeared to be amplified in double mutants (Fig. 4g). Thus, ablation of *Itgb4* may aggravate some of the defects in compact myelin organization observed in *Pmp22* mutants.

Fig. 4 Some aspects of internode architecture are altered by ablation of PMP22 and β4 integrin. (a–f) Immunolocalization of Claudin-19 (a), Kv1.1 (b) and F-Actin (a–f) in teased fibers from nerves of mice of the indicated genotypes at 30 days (a, b, d and f) and 90 days (c and e) of age. Localization of Claudin-19 at paranodes and mesaxons (a, empty arrows) and of Kv1.1 at juxtaparanodes and mesaxons (b, empty arrows) is preserved in *Pmp22* +/-, *Itgb4* SC –/– and double mutant mice at this age. While F-Actin does not accumulate in Schmidt-Lanterman incisures of animals at 1 month (d), it increases in incisures of *Pmp22* and double mutants at 3 months (c and e). In addition, F-Actin is frequently disorganized in the internodes of double mutants (c, white line). Accumulation of F-Actin in Schmidt-Lanterman incisures was analyzed by measuring the fluorescence intensity of rhodamin-labeled phalloidin, using a (d) 6 × 6 μm^2 or (e) 9 × 9 μm^2 rectangle including the entire area of every incisures. $n \geq 50$ Schmidt-Lanterman incisures per genotype (Data S1). Fluorescence was increased in *Pmp22* +/- and double mutant mice at P90. (f). Schmidt-Lanterman incisures were quantified from at least 30 internodes per genotype (Data S1). There are less Schmidt-Lanterman incisures in nerves from double mutants than in those from *Pmp22* +/- Error bars indicate SD (g) western blot analyses for p-PAK1 and PAK1 in sciatic nerves from mice at 15 and 90 days of age. *p*-PAK1 increase in *Pmp22* +/- mutants. Combined ablation of *Pmp22* and *Itgb4* increases the level of *p*-PAK1 when compared to *Pmp22* +/-. Graphs indicate mean ± SD. Statistical analyses were performed using *t*-test (e) and One-way ANOVA with Bonferroni *post hoc* test (f). $**p < 0.01$, $****p < 0.0001$.

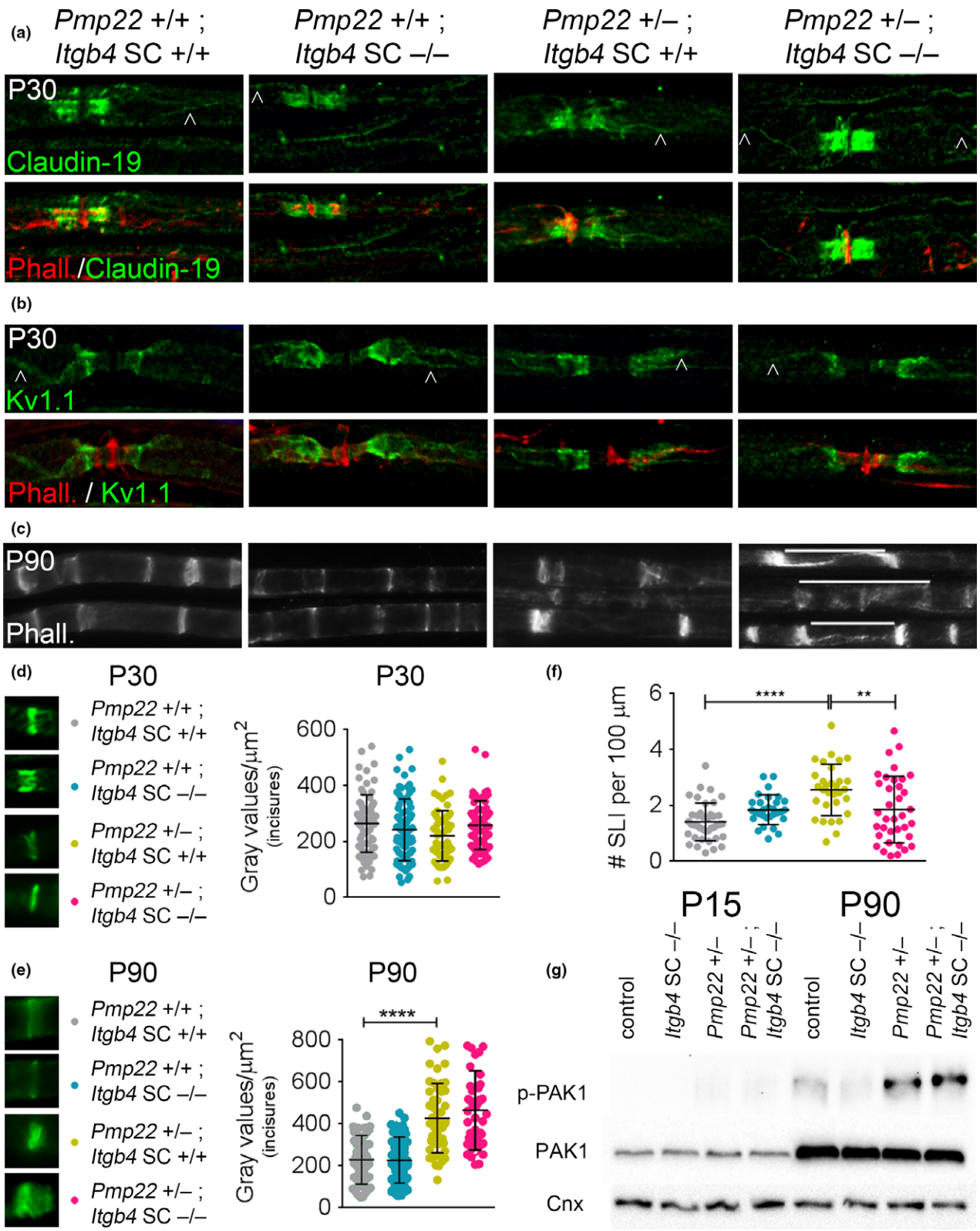
(a)
Pmp22 +/+ ; Itgb4 SC +/+
Pmp22 +/+ ; Itgb4 SC –/–
Pmp22 +/– ; Itgb4 SC +/+
Pmp22 +/– ; Itgb4 SC –/–
P30
Claudin-19
Phall./Claudin-19
(b)
P30
Kv1.1
Phall. / Kv1.1
(c)
P90
Phall.
(d)
P30
Pmp22 +/+ ; Itgb4 SC +/+
Pmp22 +/+ ; Itgb4 SC –/–
Pmp22 +/– ; Itgb4 SC +/+
Pmp22 +/– ; Itgb4 SC –/–
Gray values/µm2 (incisures)
600
400
200
0
(e)
P90
Pmp22 +/+ ; Itgb4 SC +/+
Pmp22 +/+ ; Itgb4 SC –/–
Pmp22 +/– ; Itgb4 SC +/+
Pmp22 +/– ; Itgb4 SC –/–
Gray values/µm2 (incisures)
****
800
600
400
200
0
(f)
SLI per 100 µm
****
**
6
4
2
0
(g)
P15
P90
control
Itgb4 SC –/–
Pmp22 +/–
Pmp22 +/– ; Itgb4 SC –/–
p-PAK1
PAK1
Cnx

Identification of novel partners of α6β4 integrin to further elucidate the functional interaction with PMP22

To obtain more insights in the functional interaction between α6β4 integrin and PMP22, we used mass spectrometry to identify novel proteins that immunoprecipitate with β4 integrin from sciatic nerve lysates at 30 days of age (Fig. 5a). From two independent experiments, we identified 73 candidate partners for β4 integrin. All these partners were significantly enriched in immunoprecipitates of wild-type as compared to *Itgb4* SC −/− nerves (Data S3). Among the 73 proteins, we identified several known partners of β4 integrin, including α6 integrin, vimentin,

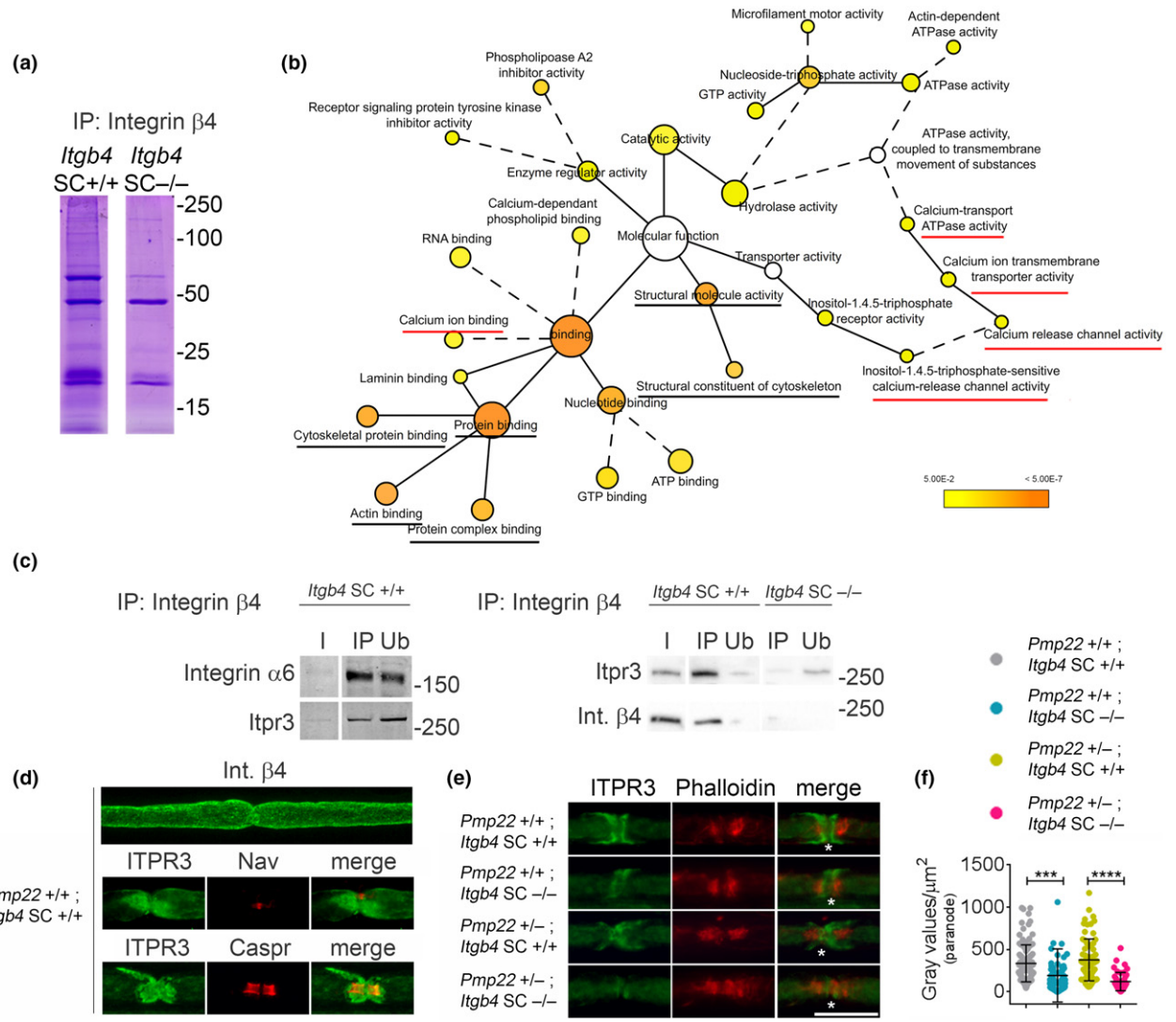

Fig. 5 β4 integrin interacts with inositol triphosphate gated calcium channel ITPR3. (a) Coomassie blue staining shows the difference between *Pmp22* +/+; *Itgb4* SC +/+ and *Pmp22* +/+; *Itgb4* SC −/− nerves after immunoprecipitation of the β4 Integrin subunit. (b) Molecular function Gene Ontology categories enriched among the partners of Integrin β4. The list of the proteins identified is shown in Data S3. Dashed lines indicated an indirect connection between two categories. (c) Immunoprecipitation of β4 integrin in *Pmp22* +/+; *Itgb4* SC +/+ and *Pmp22* +/+; *Itgb4* SC −/− sciatic nerves. The data confirm the interaction between β4 integrin and ITPR3 and the co-immunoprecipitation of the α6 integrin subunit. I = Input, IP = Immunoprecipitation and Ub = Unbound fraction. (d–f) Immunolocalization of ITPR3 in teased fibers from sciatic nerves at 30 days. Fibers were stained for β4 integrin, ITPR3, NaV, Caspr and Phalloidin. The data show that ITPR3 is enriched in the paranodal region (d). We also noticed a reduction in ITPR3 staining in the paranodes of β4 integrin mutants (e–f). Accumulation of ITPR3 at the paranode was analyzed by measuring the fluorescence intensity of ITPR3, using a 10 × 10 μm^2 rectangle including the entire area of every paranode. Scale bar, 15 μm. Nodes with adjacent tomacula were excluded from the analysis. n = 44–104 paranodes per genotype (Data S1). Graphs indicate mean ± SD. One-way ANOVA with Bonferroni *post hoc* test (f). ***$p < 0.001$, ****$p < 0.0001$.

plectin, and the laminin β1 subunit (Sonnenberg *et al.* 1988; Lotz *et al.* 1990; Rezniczek *et al.* 1998; Homan *et al.* 2002) (Data S3). Interestingly, we identified periaxin as a novel interactor of β4 integrin (Data S3). Both *Prx* −/− and *Pmp22* +/- sciatic nerves develop similar tomacula and manifest decreased NCVs (Gillespie *et al.* 2000; Court *et al.* 2004), making it a candidate to functionally link β4 integrin and PMP22. However, the protein levels and localization of periaxin were normal in *Pmp22* +/-; *Itgb4* SC −/− animals (data not shown).

For an overview of the molecular functions of the β4 integrin network based on this list of proteins, we used BiNGO, a software which recognizes network linkage by gene ontology (GO) hierarchy. The most highly represented terms in the molecular function GO category were binding and protein binding (Fig. 5b and Data S3). Consistent with previous reports, β4 integrin interacts with several cytoskeletal and actin-binding proteins (Fig. 5b). This could potentially explain the slight disruption of F-actin organization that we observed in *Pmp22* +/-; *Itgb4* SC −/− internodes.

A careful examination of the map shows a statistically significant enrichment of interactors linked to calcium binding and calcium transport GO categories (Fig. 5b, red underlines). Specifically, we identified two novel Ca^{2+} transporters as β4 integrin partners, namely the plasma membrane calcium-transporting ATPase 4 (*Atp2b4*) and inositol 1,4,5-trisphosphate receptor type 3 (*Itpr3*) (Fig. 5b). ITPR3 is an inositol triphosphate receptor that controls intracellular Ca^{2+} concentrations. ITPR3 is localized in the endoplasmic reticulum, but has also been detected at the plasma membrane (Kuno and Gardner 1987) and in the nucleus (Nicotera *et al.* 1990). In Schwann cells, ITPR3 is localized at the nodal/paranodal region and in Cajal bands (Martinez-Gomez and Dent 2007; Toews *et al.* 2007). Of note, PMP22 may regulate intracellular Ca^{2+} concentration, and Nobbio *et al.* (2009) have proposed that PMP22 neuropathies could be caused by calcium dysregulation To confirm that ITPR3 interacts with α6β4 integrin, we immunoprecipitated β4 integrin from wild-type nerves, and verified that ITPR3 and α6 integrin co-immunoprecipitation by western blot (Fig. 5c, left panel). In addition, the ITPR3 band was almost completely absent when the immunoprecipitation was performed from *Itgb4* SC-null nerves, which retained very low levels of β4 integrin protein, likely deriving form perineurial cells of vessels (Fig. 5c, right panel). In contrast, some Atp2b4 could still be immunoprecipitated with β4 integrin from *Itgb4* SC-null nerves (not shown) and we did not pursue Atp2b4 any further. We next examined the localization of ITPR3 in our mutants. In our hands, ITPR3 localized mainly to paranodal regions of wild-type nerves (Fig. 5d). α6β4 is present along all the outer Schwan cell membrane, including above the paranodal regions (Fig. 5d), suggesting that the two proteins co-localize and could interact in this location. Interestingly, we observed a reduction in the paranodal staining for ITPR3 in *Itgb4* SC-null nerves that became more evident in *Pmp22* +/-; *Itgb4* SC −/− double mutants (Fig. 5e–f). Thus, ablation of *Itgb4* alters the paranodal localization of ITPR3. Finally, we asked if this mislocalization of ITPR3 affects the concentration of calcium in Schwann cells. We performed a fluorometric determination of the intracellular Ca^{2+} concentration in Schwann cells co-cultured with dorsal root ganglia (DRG) neurons from *Pmp22* +/+; *Itgb4* SC +/+ and *Pmp22* +/-; *Itgb4* SC −/− animals, but we did not observe any difference (data not shown).

Discussion

There is evidence that PMP22 maintains myelin integrity, and part of PMP22 function may be mediated through its physical interaction with β4 integrin (Amici *et al.* 2006). To address the role of α6β4 integrin in PMP22 neuropathies, we genetically ablated β4 integrin in Schwann cells together with PMP22. We demonstrate that integrin α6β4 influences nerve conduction velocity in HNPP animals without affecting myelin thickness but possibly by enhancing the abnormalities in the architecture of myelinated fibers. Furthermore, a6β4 integrin delays the progression of myelin abnormalities in HNPP. Finally, we provide several lines of evidence that the effects of β4 integrin on HNPP pathophysiology are probably indirect, because integrin β4 and PMP22 do not co-localize in myelinating Schwann cells.

The role of laminin-integrin signaling in Schwann cell development has been defined in a large body of work–for review see (Monk *et al.* 2015; Feltri *et al.* 2016). Among laminin receptors, the function of α6β4 integrin is the most elusive and subtle. α6β4 integrin is localized at the abaxonal surface of myelinating SCs, where it regulates myelin maintenance, as its absence cause an anticipated appearance of myelin outfoldings at paranodes and juxtaparanodes, that is significantly worsened by additional ablation of another laminin receptor, dystroglycan (Nodari *et al.* 2008). Ablation of α6β4 integrin in Schwann cells also causes disorganization of Kv1.1 in the internodal mesaxon (Nodari *et al.* 2008), and of F-actin in HNPP non-compact myelin (this paper). This, together with the identification of a new candidate partner, ITPR3, enriched in the paranodal region of Schwann cells and with the worsened nerve conduction velocities of HNPP animals lacking β4 integrin, suggest a more general function for integrin α6β4 broadly related to the organization of the architecture of myelinated fibers. Similarly, laminins 211 and 511 are enriched in the nodal region (Occhi *et al.* 2005) and the laminin receptor dystroglycan is important for the organization of Schwann cell microvilli and the localization of axonal Na^{+} channels (Saito *et al.* 2003; Occhi *et al.* 2005; Colombelli *et al.* 2015). We postulate that the slight disorganization of non-compact myelin domains in internodes, Schmidt–Lanterman incisures and paranodes caused by ablation of *Itgb4* in

Schwann cells may exacerbate the functional defects of HNPP, where 35–45% of the nodes have abnormal myelin foldings, leading to a worsening of NCVs.

Myelin instabilities such as outfoldings and tomacula may derive from a common mechanism (Goebbels *et al.* 2012). The results of our study on PMP22 tomacula and α6β4 integrin outfoldings could be viewed as conflicting with this hypothesis, as we do not observe a worsening of myelin instabilities in animals lacking both proteins. However, we detected a novel interaction of integrin α6β4 with an inositol triphosphate receptor, ITRP3. Phosphoinositol and AKT signaling have been associated with myelin instabilities (Pereira *et al.* 2012). Thus, further studies will need to focus on the potential role of phosphoinositol receptors at nodes of Ranvier, in the regulation of Ca^{2+} concentration at the paranodes, and in the maintenance of myelin stability.

Acknowledgments and conflict of interest disclosure

This work was supported by Fondazione Telethon (GPP10007 to MLF and LW and GGP08021 to MLF) and the National Institutes of Health (NS045630 to MLF, NS096104 to LW). We thank Ueli Suter (Department of Biology, Institute of Molecular Health Sciences, ETH Zurich) for *Pmp22*-null mice, Filippo Giancotti (UT MD Anderson Cancer Center) for β4 integrin clones and 804G cell lines; Peter Brophy and Diane Sherman (Univ. of Edinburgh) for β4 integrin and periaxin antibodies, Shoichiro Tsukita (Kyoto University) for Claudin 19 antibody and Edward Hurley for semithin sections. Y.P, M.L.F designed research, analyzed and interpreted data; Y.P performed the majority of research; V.M and A.B performed mass spectrometry analysis; N.S performed electrophysiology analysis; D.Z. performed immunogold labeling; C.M., N.S, T.R. and D.V. provided technical assistance; Y.P and M.L.F wrote the manuscript. M.L.F and L.W. provided funding and scientific direction; L.W. critically reviewed the manuscript.

All experiments were conducted in compliance with the ARRIVE guidelines. The authors declare no competing financial interests.

Supporting information

Additional Supporting Information may be found online in the supporting information tab for this article:

Figure S1. PMP22 is enriched in compact myelin.

Figure S2. Immunolocalization of α6β4 integrin and PMP22 in teased fibers (a) and cross sections (b) from sciatic nerve at 30 days of age.

Figure S3. *Pmp22* haploinsufficiency does not affect basal lamina receptor expression or localization.

Figure S4. Immunolocalization of PMP22 in cross sections of *Pmp22*+/+ and *Pmp22*−/− sciatic nerves.

Figure S5. Flowchart of the experimental procedures.

Data S1. Sample type and size for the described experiments.

Data S2. β4 integrin and PMP22 do not co-localize in myelinating Schwann cells.

Data S3. Interactome of Integrin β4 subunit in sciatic nerve.

References

Adlkofer K., Martini R., Aguzzi A., Zielasek J., Toyka K. V. and Suter U. (1995) Hypermyelination and demyelinating peripheral neuropathy in Pmp22-deficient mice. *Nat. Genet.* **11**, 274–280.

Adlkofer K., Frei R., Neuberg D. H., Zielasek J., Toyka K. V. and Suter U. (1997) Heterozygous peripheral myelin protein 22-deficient mice are affected by a progressive demyelinating tomaculous neuropathy. *J. Neurosci.* **17**, 4662–4671.

Amici S. A., Dunn W. A., Jr, Murphy A. J., Adams N. C., Gale N. W., Valenzuela D. M., Yancopoulos G. D. and Notterpek L. (2006) Peripheral myelin protein 22 is in complex with alpha6beta4 integrin, and its absence alters the Schwann cell basal lamina. *J. Neurosci.* **26**, 1179–1189.

Amici S. A., Dunn W. A., Jr and Notterpek L. (2007) Developmental abnormalities in the nerves of peripheral myelin protein 22-deficient mice. *J. Neurosci. Res.* **85**, 238–249.

Bai Y., Zhang X., Katona I., Saporta M. A., Shy M. E., O'Malley H. A., Isom L. L., Suter U. and Li J. (2010) Conduction block in PMP22 deficiency. *J. Neurosci.* **30**, 600–608.

Chance P. F., Alderson M. K., Leppig K. A. *et al.* (1993) DNA deletion associated with hereditary neuropathy with liability to pressure palsies. *Cell* **72**, 143–151.

Coetzee T., Fujita N., Dupree J., Shi R., Blight A., Suzuki K., Suzuki K. and Popko B. (1996) Myelination in the absence of galactocerebroside and sulfatide: normal structure with abnormal function and regional instability. *Cell* **86**, 209–219.

Colombelli C., Palmisano M., Eshed-Eisenbach Y. *et al.* (2015) Perlecan is recruited by dystroglycan to nodes of Ranvier and binds the clustering molecule gliomedin. *J. Cell Biol.* **208**, 313–329.

Court F. A., Sherman D. L., Pratt T., Garry E. M., Ribchester R. R., Cottrell D. F., Fleetwood-Walker S. M. and Brophy P. J. (2004) Restricted growth of Schwann cells lacking Cajal bands slows conduction in myelinated nerves. *Nature* **431**, 191–195.

Cox J. and Mann M. (2008) MaxQuant enables high peptide identification rates, individualized p.p.b.-range mass accuracies and proteome-wide protein quantification. *Nat. Biotechnol.* **26**, 1367–1372.

Dupree J. L., Coetzee T., Blight A., Suzuki K. and Popko B. (1998) Myelin galactolipids are essential for proper node of Ranvier formation in the CNS. *J. Neurosci.* **18**, 1642–1649.

D'Urso D., Ehrhardt P. and Muller H. W. (1999) Peripheral myelin protein 22 and protein zero: a novel association in peripheral nervous system myelin. *J. Neurosci.* **19**, 3396–3403.

Einheber S., Milner T. A., Giancotti F. and Salzer J. L. (1993) Axonal regulation of Schwann cell integrin expression suggests a role for alpha 6 beta 4 in myelination. *J. Cell Biol.* **123**, 1223–1236.

Fabbretti E., Edomi P., Brancolini C. and Schneider C. (1995) Apoptotic phenotype induced by overexpression of wild-type gas3/PMP22: its relation to the demyelinating peripheral neuropathy CMT1A. *Genes Dev.* **9**, 1846–1856.

Feltri M. L., Scherer S. S., Nemni R., Kamholz J., Vogelbacker H., Scott M. O., Canal N., Quaranta V. and Wrabetz L. (1994) Beta 4 integrin expression in myelinating Schwann cells is polarized, developmentally regulated and axonally dependent. *Development* **120**, 1287–1301.

Feltri M. L., D'Antonio M., Previtali S., Fasolini M., Messing A. and Wrabetz L. (1999) P0-Cre transgenic mice for inactivation of adhesion molecules in Schwann cells. *Ann. N. Y. Acad. Sci.* **883**, 116–123.

Feltri M. L., Poitelon Y. and Previtali S. C. (2016) How schwann cells sort axons: new concepts. *Neuroscientist* **22**, 252–265.

Gillespie C. S., Sherman D. L., Fleetwood-Walker S. M. *et al.* (2000) Peripheral demyelination and neuropathic pain behavior in periaxin-deficient mice. *Neuron* **26**, 523–531.

Goebbels S., Oltrogge J. H., Wolfer S. *et al.* (2012) Genetic disruption of Pten in a novel mouse model of tomaculous neuropathy. *EMBO Mol. Med.* **4**, 486–499.

Guo J., Wang L., Zhang Y. *et al.* (2014) Abnormal junctions and permeability of myelin in PMP22-deficient nerves. *Ann. Neurol.* **75**, 255–265.

Haney C., Snipes G. J., Shooter E. M., Suter U., Garcia C., Griffin J. W. and Trapp B. D. (1996) Ultrastructural distribution of PMP22 in Charcot-Marie-Tooth disease type 1A. *J. Neuropathol. Exp. Neurol.* **55**, 290–299.

Hasse B., Bosse F., Hanenberg H. and Muller H. W. (2004) Peripheral myelin protein 22 kDa and protein zero: domain specific trans-interactions. *Mol. Cell Neurosci.* **27**, 370–378.

Homan S. M., Martinez R., Benware A. and LaFlamme S. E. (2002) Regulation of the association of alpha 6 beta 4 with vimentin intermediate filaments in endothelial cells. *Exp. Cell Res.* **281**, 107–114.

Hu B., Arpag S., Zhang X. *et al.* (2016) Tuning PAK Activity to Rescue Abnormal Myelin Permeability in HNPP. *PLoS Genet.* **12**, e1006290.

Kuno M. and Gardner P. (1987) Ion channels activated by inositol 1,4,5-trisphosphate in plasma membrane of human T-lymphocytes. *Nature* **326**, 301–304.

Lee S., Amici S., Tavori H., Zeng W. M., Freeland S., Fazio S. and Notterpek L. (2014) PMP22 is critical for actin-mediated cellular functions and for establishing lipid rafts. *J. Neurosci.* **34**, 16140–16152.

Li J. (2015) Molecular regulators of nerve conduction - Lessons from inherited neuropathies and rodent genetic models. *Exp Neurol*. **267**, 209–18.

Lotz M. M., Korzelius C. A. and Mercurio A. M. (1990) Human colon carcinoma cells use multiple receptors to adhere to laminin: involvement of alpha 6 beta 4 and alpha 2 beta 1 integrins. *Cell Regul.* **1**, 249–257.

Martinez-Gomez A. and Dent M. A. (2007) Expression of IP3 receptor isoforms at the nodes of Ranvier in rat sciatic nerve. *NeuroReport* **18**, 447–450.

Miyamoto T., Morita K., Takemoto D. *et al.* (2005) Tight junctions in Schwann cells of peripheral myelinated axons: a lesson from claudin-19-deficient mice. *J. Cell Biol.* **169**, 527–538.

Monk K. R., Feltri M. L. and Taveggia C. (2015) New insights on Schwann cell development. *Glia* **63**, 1376–1393.

Nicotera P., Orrenius S., Nilsson T. and Berggren P. O. (1990) An inositol 1,4,5-trisphosphate-sensitive Ca2 + pool in liver nuclei. *Proc. Natl Acad. Sci. USA* **87**, 6858–6862.

Nobbio L., Sturla L., Fiorese F. *et al.* (2009) P2X7-mediated increased intracellular calcium causes functional derangement in Schwann cells from rats with CMT1A neuropathy. *J. Biol. Chem.* **284**, 23146–23158.

Nodari A., Previtali S. C., Dati G. *et al.* (2008) Alpha6beta4 integrin and dystroglycan cooperate to stabilize the myelin sheath. *J. Neurosci.* **28**, 6714–6719.

Occhi S., Zambroni D., Del Carro U. *et al.* (2005) Both laminin and Schwann cell dystroglycan are necessary for proper clustering of sodium channels at nodes of Ranvier. *J. Neurosci.* **25**, 9418–9427.

Olsen J. V., de Godoy L. M., Li G. *et al.* (2005) Parts per million mass accuracy on an Orbitrap mass spectrometer via lock mass injection into a C-trap. *Mol. Cell Proteomics* **4**, 2010–2021.

Pereira J. A., Lebrun-Julien F. and Suter U. (2012) Molecular mechanisms regulating myelination in the peripheral nervous system. *Trends Neurosci.* **35**, 123–134.

Poitelon Y., Bogni S., Matafora V. *et al.* (2015) Spatial mapping of juxtacrine axo-glial interactions identifies novel molecules in peripheral myelination. *Nat. Commun.* **6**, 8303.

Quattrini A., Previtali S., Feltri M. L., Canal N., Nemni R. and Wrabetz L. (1996) Beta 4 integrin and other Schwann cell markers in axonal neuropathy. *Glia* **17**, 294–306.

Rappsilber J., Mann M. and Ishihama Y. (2007) Protocol for micro-purification, enrichment, pre-fractionation and storage of peptides for proteomics using StageTips. *Nat. Protoc.* **2**, 1896–1906.

Rezniczek G. A., de Pereda J. M., Reipert S. and Wiche G. (1998) Linking integrin alpha6beta4-based cell adhesion to the intermediate filament cytoskeleton: direct interaction between the beta4 subunit and plectin at multiple molecular sites. *J. Cell Biol.* **141**, 209–225.

Saito F., Moore S. A., Barresi R. *et al.* (2003) Unique role of dystroglycan in peripheral nerve myelination, nodal structure, and sodium channel stabilization. *Neuron* **38**, 747–758.

Sancho S., Young P. and Suter U. (2001) Regulation of Schwann cell proliferation and apoptosis in PMP22-deficient mice and mouse models of Charcot-Marie-Tooth disease type 1A. *Brain* **124**, 2177–2187.

Sherman D. L., Tait S., Melrose S. *et al.* (2005) Neurofascins are required to establish axonal domains for saltatory conduction. *Neuron* **48**, 737–742.

Snipes G. J., Suter U., Welcher A. A. and Shooter E. M. (1992) Characterization of a novel peripheral nervous system myelin protein (PMP-22/SR13). *J. Cell Biol.* **117**, 225–238.

Sonnenberg A., Modderman P. W. and Hogervorst F. (1988) Laminin receptor on platelets is the integrin VLA-6. *Nature* **336**, 487–489.

Spinardi L., Ren Y. L., Sanders R. and Giancotti F. G. (1993) The beta 4 subunit cytoplasmic domain mediates the interaction of alpha 6 beta 4 integrin with the cytoskeleton of hemidesmosomes. *Mol. Biol. Cell* **4**, 871–884.

Toews J. C., Schram V., Weerth S. H., Mignery G. A. and Russell J. T. (2007) Signaling proteins in the axoglial apparatus of sciatic nerve nodes of Ranvier. *Glia* **55**, 202–213.

Welcher A. A., Suter U., De Leon M., Snipes G. J. and Shooter E. M. (1991) A myelin protein is encoded by the homologue of a growth arrest-specific gene. *Proc. Natl Acad. Sci. USA* **88**, 7195–7199.

Yin X., Kidd G. J., Wrabetz L., Feltri M. L., Messing A. and Trapp B. D. (2000) Schwann cell myelination requires timely and precise targeting of P(0) protein. *J. Cell Biol.* **148**, 1009–1020.